Performance optimization of three-dimensional optoelectronic interconnection for intra-multi-chip-module clock signal distribution

Chunhe Zhao and Ray T. Chen

Microelectronics Research Center
The University of Texas at Austin, Austin, TX 78712

ABSTRACT

The structure, fabrication and theory of a three-dimensional (3-D) planarized optoelectronic clock signal distribution device, based on a thin light-guiding substrate in conjunction with a 2-D polymer holographic grating array, are described. We have previously demonstrated a 25 GHz 1-to-42 (6×7) highly parallel fanout interconnect with a signal to noise ratio of 10 dB[1]. In this letter, theoretical work focused on generating a globally uniform fanout distribution is presented. An objective function aimed at equalizing the intensities among the fanout beams is established and optimization results are reported. Finally, the angular misalignment and wavelength dispersion problem are further discussed, together with their tolerance requirements on the size of the photoreceivers and the bandwidth of the vertical cavity surface emitting lasers integrated on the multi-chip-modules (MCMs).

Keywords: optical interconnection; clock signal distribution; holographic gratings; diffraction efficiency.

1. INTRODUCTION

The evolution of the integrated circuit technology from VLSI to ULSI has led to the increases in both the system size and operation speed. As a result, system clock skew and data transfer rate become major concerns in implementing high speed system[1]. Multi-chip-module (MCM) is employed to provide higher clock speeds and circuit densities through minimizing the chip-to-chip interconnection distance. It is still difficult, however, to electrically distribute synchronous clock signals to the GHz region in intra-MCM and inter-MCM levels due to the required large fanout, the associated skin effect and long interconnection path.

Optical interconnections, on the other hand, outperform electrical interconnections in these scenarios, due to their performance advantages of speed and frequency-independent loss feature. We recently reported a unique three-dimensional (3-D) free-space compact optical parallel fanout interconnect for massive clock signal distribution, which, when integrated with vertical cavity surface emitting lasers (VCSEL) and photoreceivers, can be used for intra- and inter-MCM interconnects[1]. Because of the 3-D interconnection feature of the reported device, it minimizes the employment of the real estate of the semiconductor surface, which is pivotal for a miniaturized massive fanout interconnect system using planar integration technology. More importantly, the parallel feature of the fanout beams and the planarized compact device structure convert the unsolved 3-D spatial and angular multiple alignment problem into a single 2-D planar step, which greatly eases the packaging difficulties. The physical structure of such a clock signal distribution device[1] employed a thin light-guiding plate and was integrated with a 2-D holographic grating array on its surface. In the previous experiment, a thin glass plate was employed as the light guiding medium. Fabrication of this device required the formation of a photopolymer layer[4] on the surface of the waveguiding plate. Arrays of holographic gratings were recorded afterward[5]. One of the most pivotal issues to make this device useful for high-performance system is to provide the 1-to-many (many=42 in previous paper) fanouts with an equal power. The power fluctuation among the 42 fanout beams in the previous paper is as high as 25 dB[1] which makes the subsequent optical to electrical conversion impractical when considering the preset logic levels associated with. In this paper, we present the theory needed to maintain equal fanouts among all 42

0-8194-2004-2/95/$6.00

beams.

2. BRAGG DIFFRACTION ANALYSIS

Fig. 1 shows a portion of the device configuration containing a section of the microstructure of the holographic grating arrays attached to the waveguiding plate we previously reported[1]. The optical signal propagation inside the device is also portrayed. In this figure, the $\bar{K}_{ij}^{v}$'s (v=x or y; i=1, ..., 6; j=1 for v=x and j=1, ..., 7 for v=y) are the grating vectors recorded in the photopolymer, the $\bar{k}$ and $\bar{k}'$'s are the incident and diffracted wave vectors, and the sub- or superscript x's (y's) represent light beams or grating vectors along x (y) direction. For Bragg diffraction, we have

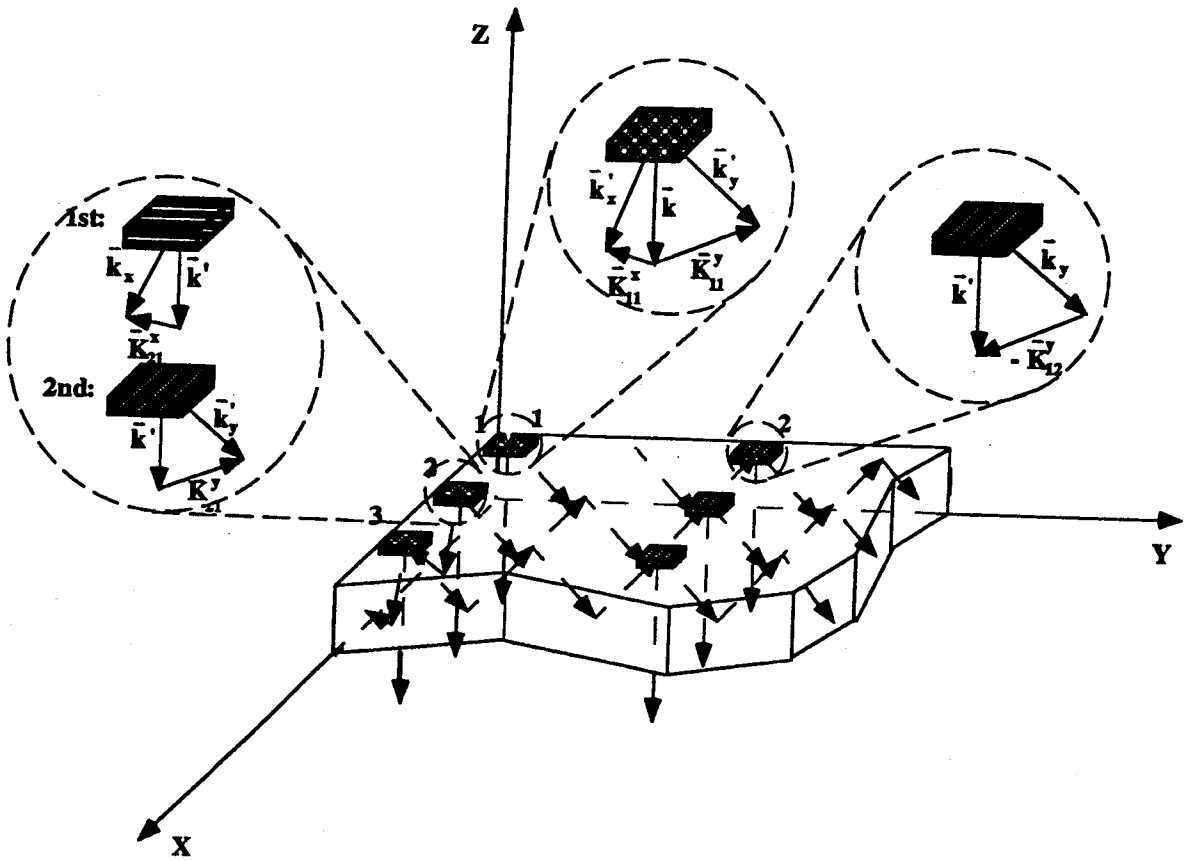

Fig. 1. Device configuration for free-space optoelectrnic interconnection. The enlarged portions show the phase-matching conditions at three typical holographic grating sites.

$$\bar{k}' = \bar{k} - \bar{K}. \tag{1}$$

The phase-matching condition for the three representative planarized gratings of the device are clearly shown in Fig. 1, where we have labeled the locations of the planarized gratings using two subscripts. The first is the position in the x direction and the second in the y direction. The sites with denotation (i,1) (i=1, ..., M, where M is the number of "rows" of planarized grating sites on the device) have two multiplexed holograms with grating vectors $\bar{K}_{i1}^{x}$ and $\bar{K}_{i1}^{y}$, respectively, while the subscript (i,j) (i=1, ..., M; j=2, ..., N, and N is the number of "columns ") represents location with only one planarized grating vector $\bar{K}_{ij}^{y}$. The first planarized multiplexed grating (1,1) is designed as an input coupler which couples

the surface-normal input laser beam $\bar{k}$ into two substrate guided beams $\bar{k}_x'$ and $\bar{k}_y'$, with bouncing angles θ_x and θ_y greater than the total internal reflection angle, and propagating along x and y directions, respectively.

Once propagating to the subsequent planarized grating at site (1,2), the input substrate guided beam $\bar{k}_y'$ is partially coupled surface-normally out of the device into $\bar{k}'$ by the grating $\bar{K}_{12}^{y}$. At the location of (2,1), the input substrate guided beam $\bar{k}_x'$ is first partially coupled into a surface-normal light beam $\bar{k}'$ by the grating $\bar{K}_{21}^{x}$, and then $\bar{k}'$ is partially coupled into $\bar{k}_y'$ by grating $\bar{K}_{21}^{y}$, and then propagates along y direction. Similar consideration is applicable to the remaining holographic grating sites. Every time the coupling efficiency is not designed at 100%. It is clear from the above analysis that a 3-D free-space surface-normal parallel fanout interconnect is constructed by the 2-D planarized grating arrays.

3. PERFORMANCE OPTIMIZATION

The system power budget for such a high speed fanout device is limited by the channel with the weakest fanout intensity. Power uniformity is therefore crucial in the system design involving massive cascaded fanouts. For the optical clock signal distribution described herein, the power of input optical signal is always limited by the output channel with the lowest fanout intensity among the $M \times N$ fanout beams. To optimize the performance of our device, aimed at providing a uniform fanout intensity distribution, we define a transmission function, which is the power of the substrate guided light beam transmitted from one hologram to the next. To simplify our calculation, we assume a unit input power. The transmission functions associated with the first column of multiplexed holographic gratings shown in Fig. 1 can be represented by

$$\begin{aligned} T_2^x &= \eta_1^x, \\ T_i^x &= T_{i-1}^x\left(1-\eta_{i-1}^x\right) \quad (i = 3, \ldots, M), \end{aligned} \tag{2}$$

where T_i^x (i=2, ..., M) is the power of light beam transmitted onto grating (i,1) from grating (i-1,1) along x direction and η_{i-1}^x (i=1, ..., M) is the diffraction efficiency of the planarized gratings which couple the light beam out of or into the device along x direction. The multiplexed planarized gratings in column 1 couple the light beams propagating in x direction onto the second column, so the transmission functions can be written as

$$\begin{aligned} T_{12}^y &= \eta_{11}^y, \\ T_{i2}^y &= T_i^x \eta_i^x \eta_{i1}^y \quad (i = 2, \ldots, M). \end{aligned} \tag{3}$$

Similar to above, here T_{i2}^y (i=1, ..., M) means the intensity of the light beam transmitted to location (i,2), and η_{i1}^y (i=1, ..., M) is the diffraction efficiency of the grating at location (i,1). Finally, for the rest of the planarized gratings, the transmission functions can easily be written as

$$T_{ij}^y = T_{i,j-1}^y\left(1-\eta_{i,j-1}^y\right) \quad (i = 1, \ldots, M;\ j = 3, \ldots, N). \tag{4}$$

After we have derived the transmission functions, the expressions for the fanout intensities P_{ij}'s (i=1, ..., M; j=1, ..., N) can be obtained by tracing the flow of optical energy from the input coupler (1,1) to the desired location (i,j), which are

$$
\begin{aligned}
P_{11} &= 1-\eta_1^x-\eta_{11}^y, \\
P_{i1} &= T_i^x\eta_i^x\left(1-\eta_{i1}^y\right)\ (i=2,\ ...,\ M), \\
P_{ij} &= T_{ij}^y\eta_{ij}^y\ (i=1,\ ...,\ M;\ j-2,\ ...,\ N).
\end{aligned} \tag{5}
$$

Optimization of the performance of our device is to find an optimized distribution of diffraction efficiencies which will lead to a fanout intensity distribution with a minimum power fluctuation and therefore an optimized power budget. For this purpose, an objective function[6] relating all terms of power fluctuations is generated. By optimizing the objective function, a uniform fanout intensity distribution can be reached. For our problem, an obvious objective function is the sum of the square values of the differences between the fanout intensities and their average[6]. Base on the above assumption, for our device with $M\times N$ fanout beams, the average intensity is

$$
\overline{P}=\frac{1}{M\times N}. \tag{6}
$$

The objective function is then expressed as

$$
E=E_1+E_2, \tag{7}
$$

where

$$
\begin{cases}
E_1=\sum_{i=1}^{M}\sum_{j=1}^{N}\left(\frac{P_{ij}}{\overline{P}}-1\right)^2 & \text{for } P_{ij}\ge\overline{P}\ (i=1,\ ...,\ M;\ j=1,\ ...,\ N), \\
E_2=\sum_{i=1}^{M}\sum_{j=1}^{N}\left(\frac{\overline{P}}{P_{ij}}-1\right)^2 & \text{for } P_{ij}<\overline{P}\ (i=1,\ ...,\ M;\ j=1,\ ...,\ N).
\end{cases} \tag{8}
$$

To minimize the power consumption of our device, we must have

$$
\eta_M^x=1,\ \eta_{iN}^y=1\ (i=1,\ ...,\ M), \tag{9}
$$

for the outest linear arrays where all energy is coupled out surface-normally. To this point, the total number of unknown η's is $(M-1)+(M\times N-M)=M\times N-1$. The optimization process is carried out by minimizing the objective function E with respect to these $M\times N-1$ η's. Note that the results derived through this calculation is applicable to any integer combination of M and N. In accordance with our previous work[1], we provide the result for M=6 and N=7. In Table 1 (next page) we summarize the optimized diffraction efficiency distribution for an equalized fanout intensity of 0.0238 (1/42) per channel (Eq. 6). This result is further illustrated in Fig. 2 (next page), where the black bars are for η_i^x's (i=1, ..., M) and others for η_{ij}^y's (i=1, ..., M; j=1, ..., N), and the two-section structure at y=1 and x=1, ..., 6 clearly shows the diffraction efficiencies of a linear array of multiplexed holographic gratings. The diffraction efficiency of the polymer holographic gratings can be accurately controlled experimentally[5], and diffraction efficiencies as high as 100% can be reached[7]. It is clear from Table 1 and Fig. 2 that, for an arbitrary $M\times N$ fanouts, there're M+N+1 sets of holograms with different diffraction efficiencies along x and y directions, respectively. For the specific case demonstrated[1], M=6 and N=7, we need 14 sets of holograms to provide the required equal fanouts. Table 1 also indicates that, for an arbitrary matrix of $M\times N$, beginning from the 2nd row, the values of η_i^x's (i=2, ..., M) varies as

η_{ij} y / x	1		2	3	4	5	6	7
	η_{i1}^{x} ⊗	η_{i1}^{y} ⊖	Ⓨ	Ⓨ	Ⓨ	Ⓨ	Ⓨ	Ⓨ
1	0.833	0.143	0.167	0.200	0.250	0.333	0.500	1.000
2	0.200	0.857	0.167	0.200	0.250	0.333	0.500	1.000
3	0.250	0.857	0.167	0.200	0.250	0.333	0.500	1.000
4	0.333	0.857	0.167	0.200	0.250	0.333	0.500	1.000
5	0.500	0.857	0.167	0.200	0.250	0.333	0.500	1.000
6	1.000	0.857	0.167	0.200	0.250	0.333	0.500	1.000

Table 1. Optimized diffraction efficiency distribution for uniform fanout distribution for the case M=6, N=7. The symbol ⊗ means that the holographic gratings in that column couple light beam propagating along x direction surface-normally out of the substrate, Ⓨ means that gratings in that column couple light propagating along y direction surface-normally out of the substrate and ⊖ means that gratings in that column couple light into y direction.

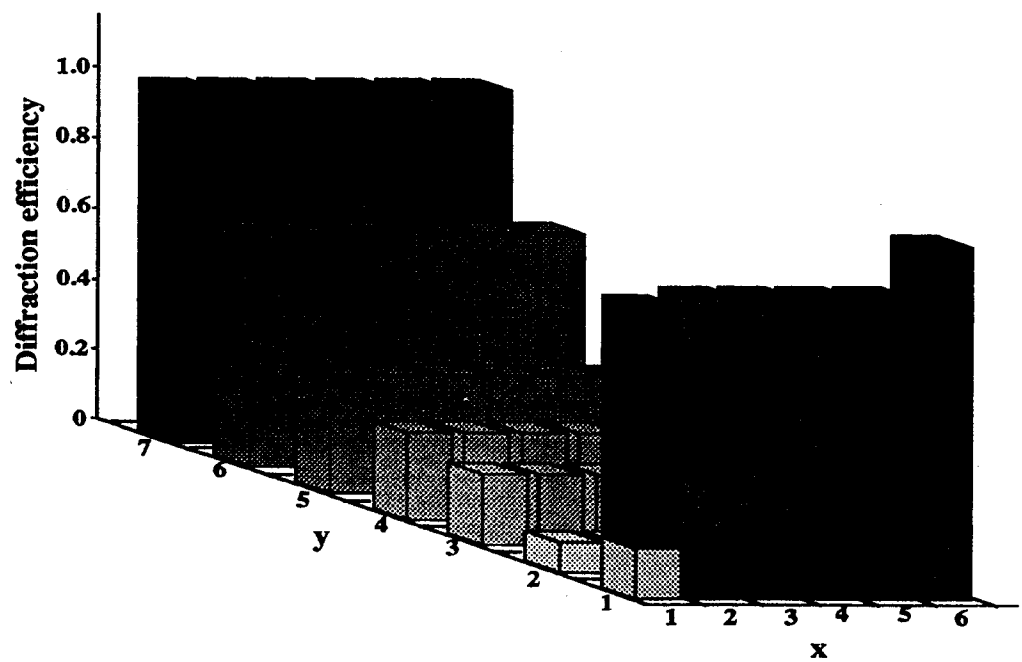

Fig. 2. Optimized diffraction efficiency distribution for uniform fanout distribution for the case M=6, N=7. The red bats are for η_i^x's (i=1, ..., M) and the bars filled with other colors are for η_{ij}^y's (i=1, ..., M; j=1, ..., N).

$$\eta_i^x = \frac{1}{M+1-x} \quad (i = x = 2, \ldots, M), \tag{10}$$

where x is the location of the hologram along x direction. The same reciprocal relation is also valid for η_{ij}^y's (1=1, j=1 and i=1, ..., M, j=2, ..., N) along y direction, i.e.,

$$\eta_{ij}^y = \frac{1}{N+1-y} \quad (i = 1, j = y = 1;\ i = 1, \ldots, M,\ j = y = 2, \ldots, N). \tag{11}$$

Experimentally, the above observation can be used in the recording of the holographic grating to greatly reduce the degree of complexity. By precisely controlling the diffraction efficiencies of the holographic grating arrays according to our optimized result, a uniform fanout intensity distribution can be attained.

The clock skew associated with the device we investigated here can be calculated by considering the longest path the clock signal travels inside the wave guiding plate, which is the path between the input coupler at location (1,1) and the output coupler at (6,7). If we assume a light beam bouncing angle of $\gamma = 45°$ and a substrate thickness of d = 1 mm as shown in Fig. 3, this longest light path would be

$$l = \frac{2d}{\cos\gamma} \times [(6-1)+(7-1)] = 3.1 \text{ cm}. \tag{12}$$

So, the largest clock skew incurred by the planar clock distribution of the device is

$$t_{Skew} = \frac{l}{c/n} = 150 \text{ psec}, \tag{13}$$

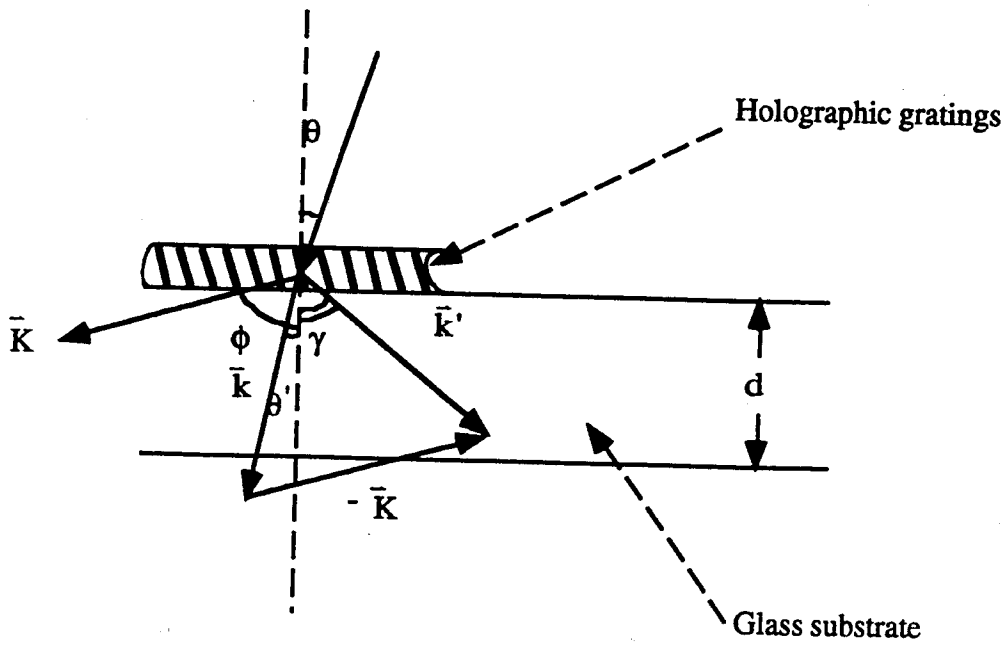

substrate.

Fig. 3. Propagation vectors of the input and diffracted beams, and their relation to the grating vector $\bar{K}$, for an 1-D array of holographic gratings.

4. ALIGNMENT CONSIDERATION

Several factors will affect the alignment and the coupling efficiency of our device when integrated with other circuits. First is the angular misalignment of the input beam. Fig. 3 shows the phase-matching condition of a hologram for surface-normal coupling. For Bragg diffraction, we have[8]

$$\begin{pmatrix} -\sin\gamma \\ \cos\gamma \end{pmatrix} = \begin{pmatrix} \dfrac{\sin\theta}{n} - \dfrac{K}{\beta}\sin\phi \\ \sqrt{1 - \dfrac{\sin^2\theta}{n^2}} - \dfrac{K}{\beta}\cos\phi \end{pmatrix}, \tag{14}$$

where n is the refraction index of the hologram and $\beta = 2\pi n/\lambda$ is the propagation constant of light with wavelength λ. After eliminating ϕ from Eq. (14) and differentiating the resulting equation, we have

$$\Delta\gamma = \frac{\left[\sin\theta - n\left(\dfrac{K^2}{2\beta^2} - 1\right)\sin\gamma\right]\cos\theta}{\left[\left(\dfrac{K^2}{2\beta^2} - 1\right)\sin\theta - n\sin\gamma\right]n\cos\gamma}\Delta\theta. \tag{15}$$

If we assume that the number of total internal reflection of the specific light beam shown in Fig. 3 is m, then the corresponding device length is

$$L = md\tan\gamma. \tag{16}$$

From Eqs. (15) and (16), a variation of the angle of the input light beam will lead to a spatial shift of the fanout beam on the device surface of

$$\Delta L = \frac{\left[\tan(\gamma + \Delta\gamma) - \tan\gamma\right]}{\tan\gamma}L, \tag{17}$$

and $\Delta\gamma$ is given by Eq. (15). This relation is schematically shown in Fig. 4 (see next page). In our calculation, we have assumed the wavelength of the VCSEL as $\lambda = 850$ nm, n=1.512 (polymer waveguide), $\theta = 0°$ (surface-normal), $\gamma = 45°$ and L is taken as the longest distance, that is $(2d\tan\gamma)\times[(6-1)+(7-1)] = 2.2$ cm. We see from Fig. 4 that within a small angular misalignment of the input light beam, ΔL changes linearly with $\Delta\theta$, which can also be seen from Eqs. (15) and (17).

Another factor that affects the alignment and the coupling efficiency of the 1-to-many massive fanout devices is the spectral width of the input laser beam. Large spectral width in the input light will lead to a deviation of diffraction from Bragg condition, which will result in a spreading of the size of the fanout beam. In fact this mechanism has been used in the design of a wavelength division demultiplexing (WDDM) device[9]. Currently the line width of emission from VCSEL can be as narrow as less than 1 Å, according to the theory in Ref. 9, this gives rise to a ~ 4.3 μm spatial shift of the output beam.

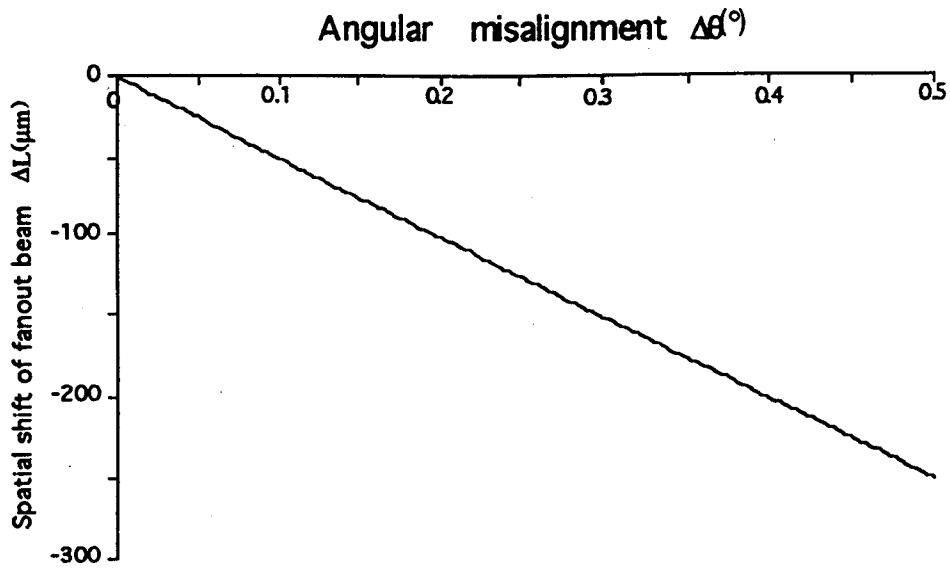

Fig. 4. Variation of spatial position of fanout beam on the device surface with respect of the input light beam angular misalignment.

5. CONCLUSIONS

In this paper, we present the theory of the intensity optimization of a massive fanout optical clock signal distribution, based on a 1 mm light-guiding substrate in conjunction with 2-D planarized holographic grating arrays. The theoretical result shows that a uniform fanout intensity distribution exists. Such an optimized condition among $M \times N$ fanouts can be attained through precisely controlling the diffraction efficiencies of the holographic gratings according to the optimized results. Reciprocal relationship of the diffraction efficiencies with their position along x and y directions are observed which, if applied in the process of recording of the holographic gratings, would greatly reduce the degree of complexity. Clock skew problem associated with the demonstrated device is studied and a clock skew of 150 psec is obtained. Further packaging-related parameters such as angular misalignment and wavelength dispersion are also discussed.

This research is sponsored by Cray Research and APAR's Center of Optoelectronics Science and Technology.

6. REFERENCES

1. Suning Tang and Ray T. Chen, "1-to-42 optoelectronic interconnection for intra-multichip-module clock signal distribution," *Appl. Phys. Lett.*, vol. 66, no. 22, 2931(1994).
2. M. Afghahi and C. Svensson, "Performance of Synchronous and Asynchronous Schemes for VLSI Systems," *IEEE Trans. Comput.*, vol. 41, no. 7, 858(1992).
3. H. P. Herzig and R. Dandliker, "Diffractive components: holographic optical elements," in *Perspectives for Parallel Optical Interconnects*, P. Lalanne and P. Chavel, ed., Springier-Verlag, New York(1993).
4. W. J. Gambogi, A. M. Weber and T. J. Trout, "Advances and Applications of Dupont Holographic Photopolymer," *Proc. SPIE*, vol. 2043, 2(1993).
5. Ray T. Chen, H. Lu, D. Robinson, M. Wang, G. Savant and T. Jannson, "Guided-Wave Planar Optical Interconnects Using Highly Multiplexed Polymer Waveguide Holograms," *J. Lightwave Tech.*, vol. 10, no. 7, 888(1992).
6. K. W. Cattermole and J. J. O'Reilly, *Optimization Methods in Electronics and Communication*, New

York: Wiley(1984).
7. L. H. Lin, "Hologram Formation in Hardened Dichromated Gelatin Films," *Applied Optics*, vol. 8, no. 5, 963(1969).
8. H. Kogelnik, "Coupled Wave Theory for Thick Hologram Gratings," *The Bell System Technical Journal*, vol. 48, no. 9, 2909(1969).
9. M. M. Li and Ray T. Chen, "Two-channel surface-normal wavelength division demultiplexer using substrate guided waves in conjunction with multiplexed waveguide holograms," *Appl. Phys. Lett.*, vol. 66, no. 3, 262(1995).